ACS APPLIED MATERIALS & INTERFACES

Research Article

www.acsami.org

Anodic, Cathodic, and Annihilation Electrochemiluminescence Emissions from Hydrophilic Conjugated Polymer Dots in Aqueous Medium

Ruiping Dai, Fanmin Wu, Huifeng Xu, and Yuwu Chi*

Ministry of Education Key Laboratory of Analysis and Detection for Food Safety, State Key Laboratory of Photocatalysis on Energy and Environment, and College of Chemistry, Fuzhou University, Fujian 350108, China

Supporting Information

ABSTRACT: Hydrophilic poly[2-methoxy-5-(2-ethylhexyloxy)-1,4-phenylenevinylene] (MEH-PPV) conjugated polymer dots (CP-dots) capped by Triton X-100 were synthesized. For the first time, the electrochemiluminescence (ECL) emission of CP-dots was investigated in aqueous solution. At the glassy carbon/water interface, the CP-dots have excellent and multichannel ECL properties, such as having annihilation ECL activity in the absence of coreactants, and give bright anodic and cathodic ECL emission (590 nm) in the presence of tri-*n*-propylamine (TPrA) and peroxydisulfate ($S_2O_8^{2-}$), respectively. The versatile ECL properties of the hydrophilic CP-dots combined with their low cytotoxicity, good biocompatibility, and easy bioconjugation may suggest promising applications of this new type of ECL nanomaterial in novel biosensing and bioimaging, and new types of light-emitting devices.

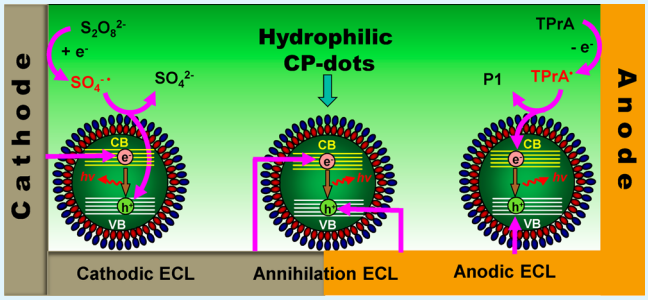

KEYWORDS: *CP-dots, electrochemiluminescence, annihilation, coreactant, Triton X-100*

1. INTRODUCTION

Conjugated polymers (also called semiconducting polymers) are promising materials for various optoelectronic applications, including light-emitting diodes, field-effect transistors, and photovoltaic devices.[1−3] Conjugated polymer dots (CP-dots) were originally developed for preparing thin film in the optoelectronic devices.[4,5] However, in recent years, CP-dots have attracted considerable attention due to their high intensity of fluorescence and good photostability.[6] Because of their outstanding characteristics, a lot of CP-dots have been used as bright fluorescence probes.[7−9] At the same time, they have exhibited low cytotoxicity and good biocompatibility compared to the heavy metal quantum dots; thus, these nanomaterials have drawn more and more attention for biological applications including bioimaging and drug delivery.[10−12]

In general, polymerization in heterophase systems and postpolymerization dispersion, including emulsion and reprecipitation techniques, are two main methods for preparing CP-dots.[13] Some CP-dots have been produced from semiconducting polymer using surfactants, such as sodium dodecyl sulfate (SDS) or poly(ethylene glycol) (PEG), as capping agents via miniemulsion methods.[14−17] Recently, some CP-dots have been synthesized from commercially available polymers by simple reprecipitation methods.[18−20] However, the lack of functional groups for commercial conjugated polymer limits the applications of CP-dots in some extent. Therefore, several strategies have been developed for synthesizing functionalized CP-dots. The main routes include cross-linking CP-dots with functional polymer molecules in reprecipitation procedures,[21−25] and synthesizing functionalized CP-dots from specially designed conjugated polymers with various functional groups.[26,27]

In addition to the applications in fluorescence sensing and imaging systems, CP-dots have been applied in the electrochemiluminescence (ECL) system. Bard and co-workers first prepared the F8BT CP-dots and investigated their ECL in the acetonitrile solution.[28] Recently, they have investigated the ECL properties of oligothiophene CP-dots in benzene/acetonitrile solution.[29,30] However, since these ECL systems work in the organic solvent, the volatile solvent vapors may do harm to the environment and experimenter, and the ECL sensing applications of CP-dots are limited due to the fact that most analytes are distributed in the aqueous solutions. Although CP-dots with strong ECL properties may have promising applications in chemical sensing, the ECL research based on the CP-dots is still in its infancy. Much research is needed for the ECL of CP-dots, especially synthesis of hydrophilic CP-dots, and their ECL behaviors and mechanisms in aqueous solutions.

Received: September 30, 2014
Accepted: June 26, 2015
Published: June 26, 2015

DOI: 10.1021/acsami.5b04305
ACS Appl. Mater. Interfaces 2015, 7, 15160−15167

In this work, stable, uniform, and hydrophilic CP-dots were synthesized by capping conjugated polymer, poly[2-methoxy-5-(2-ethylhexyloxy)-1,4-phenylenevinylene] (MEH-PPV) particles, with Triton X-100. MEH-PPV conjugated polymer was selected for the synthesis of CP-dots with ECL properties since MEH-PPV is one of the most widely studied light emitting polymers that glow when excited by electricity,[31] and MEH-PPV film has shown good ECL activities in organic solvent.[32] Triton X-100 was chosen as the capping surfactant based on the consideration that Triton X-100 is a widely used nonionic surfactant and has good solubility in the organic solvents such as benzene and tetrahydrofuran (THF) needed for dissolving MEH-PPV,[24] making it easy to obtain surfactant-capped CP-dots by the simple reprecipitation method mentioned above. For the first time, ECL of CP-dots in aqueous medium was studied. The CP-dots exhibit annihilation ECL activity upon switching potential between anodic and cathodic potentials and give bright anodic and cathodic ECL emission in the presence of tri-*n*-propylamine (TPrA) and peroxydisulfate ($S_2O_8^{2-}$), respectively. The nonsurface state ECL mechanism of the CP-dots at the glass carbon/water interface was investigated and discussed. Finally, the potential application of CP-dots in sensing was envisioned.

2. EXPERIMENTAL SECTION

Material. Poly[2-methoxy-5-(2-ethylhexyloxy)-1,4-phenylenevinylene] (MEH-PPV, average MW 70 000−100 000) was purchased from Sigma-Aldrich. Tri-*n*-propylamine (TPrA) was purchased from Fluka. Triton X-100, tetrahydrofuran (THF, anhydrous, 99.9%), potassium peroxydisulfate ($K_2S_2O_8$), phosphate (PBS buffer), and the filter membrane were available from local reagent suppliers. All other reagents employed were of analytical grade. Doubly distilled water was used throughout this work.

Preparation of Triton X-100-Capped MEH-PPV CP-Dots. The Triton X-100-capped MEH-PPV CP-dots was prepared by modifying the reprecipitation procedure for hydrophobic CP-dots reported in the literature;[20] i.e., the co-solution of conjugated polymer and Triton X-100 in tetrahydrofuran (THF) was used as the precursor instead of the pure solution of conjugated polymer in THF. In a typical procedure, 10 mg of MEH-PPV conjugated polymer was dissolved in 20 mL of THF by stirring overnight under a nitrogen atmosphere, and the solution was filtered through a filter paper to remove any insoluble material. The polymer solution was diluted and mixed with 20 μL of Triton X-100 in THF to produce an MEH-PPV concentration of 20 ppm by sonication. Then, 2 mL of the mixture was injected into 8 mL of ultrapure water under the vigorous sonication condition. The THF was removed by partial vacuum evaporation, followed by filtration through a 0.2 μm membrane filter, to obtain MEH-PPV CP-dots. The excess free Triton X-100 molecules were not removed from the CP-dot suspension since they almost did not affect the electrochemiluminescent property of CP-dots and could make the CP-dots more stable in aqueous solution. The fluorescent and electrochemiluminescent properties did not obviously change in aqueous media over a long time (more than 6 months). The hydrophilic Triton X-100-capped CP dot aqueous solution was stored in the dark at 4 °C before further usage. For a control, the hydrophobic CP-dots, i.e., MEH-PPV CP-dots without Triton X-100 capping, were prepared by the previously reported procedure.[20]

Instrumental Analysis. The fluorescence spectra of MEH-PPV CP-dots were measured using an F-4600 fluorescence spectrophotometer (Hitachi, Japan), and the excitation wavelength was set at 500 and 520 nm for MEH-PPV polymer in THF solvent and MEH-PPV CP-dots, respectively. UV−vis absorption spectra were characterized by a UV−vis spectrophotometer (TU-1950, Persee). The morphology and size of the MEH-PPV CP-dots were characterized by atomic force microscopy (AFM) with a Nanoscope Multimode IIIa (Veeco Instruments, USA) and dynamic light-scattering (DLS) technology using a ZetaPALS (Brookhaven Instrument Corporation, USA), respectively. ECL and electrochemistry were measured on an EC&ECL detection system (MPI-E, Remex Electronic Instrument Lt. Co., Xi'an, China) equipped with a working electrode (e.g., GC, Pt or Au disk electrode with a diameter of 2.0 mm), a Pt wire counter electrode, and an Ag/AgCl (3 M KCl) reference electrode. Unless otherwise stated, the biased high potential of the photomultiplier tube (i.e., PMT) was −800 V. A set of optical cutoff filters (495, 535, 555, 575, 590, 620, 640, 680, and 705 nm) were used to measure ECL spectra by being placed in turn before the PMT window during the detection of ECL intensity.

ECL Measurements of MEH-PPV CP-Dots. Before ECL measurement, the working electrode was freshly cleaned and modified with a layer of CP-dots by dropping and drying 1 μL of CP-dot aqueous solution on the electrode surface at room temperature. Annihilation ECL activity of CP-dots was investigated by applying a 1 Hz potential step between the anodic potential (+0.7 V) and the cathode potential (−1.4 V). The anodic ECL of MEH-PPV CP-dots was measured by applying an anodically polarized potential from 0 to +1.3 V at a scan rate of 100 mV/s in the absence and presence of TPrA. The cathodic ECL of MEH-PPV CP-dots was measured by applying a cathodically polarized potential from 0 to −1.5 V at a scan rate of 100 mV/s in the absence and presence of $K_2S_2O_8$.

3. RESULTS AND DISCUSSION

Morphology and Spectrum Characterization of Hydrophilic MEH-PPV CP-Dots. The AFM image of the hydrophilic CP-dots is shown in section (a) of Figure 1A. From the typical height profile along the line plotted in the AFM image (section (b) in Figure 1A), and the related size

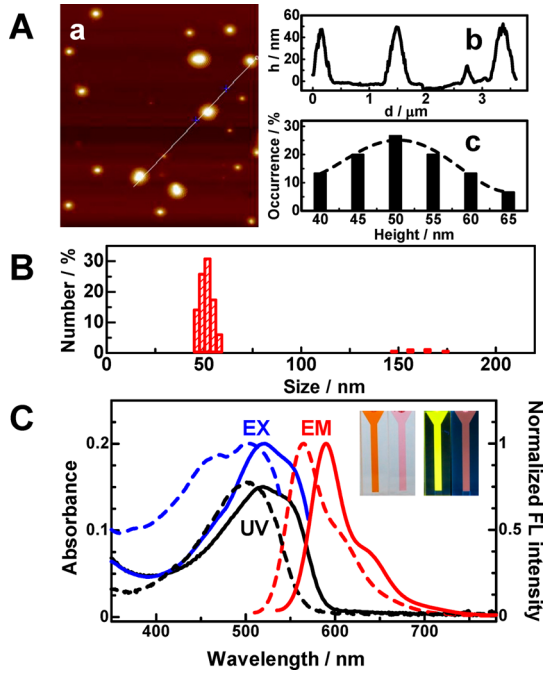

Figure 1. (A) AFM data of Triton X-100-capped MEH-PPV CP-dots: (a) AFM image; (b) the height profile along the line plotted in AFM image; (c) height distribution. (B) Size distribution obtained for CP-dots by DLS. (C) UV−vis absorption (black line), fluorescence emission (red line), and fluorescence excitation spectra (blue line) of MEH-PPV polymer in THF solvent (dashed line) and MEH-PPV CP-dots in aqueous solution (solid line). Inset: first and second from the left are, respectively, the photos of MEH-PPV polymer in THF and CP-dots in water under white light; first and second from right are, respectively, the photos of CP-dots in water and MEH-PPV polymer in THF under 365 nm UV light.

DOI: 10.1021/acsami.5b04305
ACS Appl. Mater. Interfaces 2015, 7, 15160−15167

distribution (section (c) in Figure 1A), it can be known that the hydrophilic CP-dots exhibit a relatively narrow distribution with an average height of 50 nm. The DLS data shown in Figure 1B suggest that the size distribution column of hydrophilic CP-dots is centered at 50 nm with a quite narrow shape. The DLS result is well consistent with that of AFM in particle size.

For a better understanding of the optical and electrochemical properties, it is necessary to analyze the structure of Triton X-100 functionalized CP-dots and answer the question of whether Triton-X 100 was coated on the MEH-PPV dot surfaces or was just blended inside the MEH-PPV dot matrix. The synthesized Triton X-100 modified CP-dots were dialyzed by a 10000 Da MWCO membrane, allowing the removal of Triton X-100 (with a molecular weight of 647 Da) from the Triton X-100-CP-dot system while keeping CP-dots (>70 000 Da). If Triton-X 100 was coated on the surfaces of CP-dots, then the size of CP-dots would not change significantly. Otherwise, if Triton X-100 was just blended inside the CP-dot matrix, then the CP-dots might be divided into much smaller particles due to the interaction of the blended Triton X-100 with water and the separation of MEH-PPV chains along the places occupied by Triton X-100. The dialysis experimental result shows that the size of Triton X-100 modified CP-dots was changed from 50 to 44 nm (Figure S1, Supporting Information). The slight change in diameter of the particles indicates that Triton-X 100 was coated at the surfaces of CP-dots. The sizes of core−shell structures and encapsulation efficiency of Triton X-100 on the CP-dots was approximately estimated from the amount of Triton X-100 immobilized on the CP-dots after completely removing free Triton X-100 by long time dialysis (see Figure S2 and related data analysis in the Supporting Information). The core size of the hydrophilic CP-dots was approximately estimated to be 35 nm (ca. 160 MEH-PPV chains). The thickness of Triton X-100 shells of the CP-dots were, respectively, 7.5 nm (ca. two-molecule-layer thick) and 4.5 nm (ca. one-molecule-layer thick) before and after dialysis (Figure S3, Supporting Information). The hydrophilic CP-dots after dialysis (44 nm in diameter) was likely coated with one Triton X-100 layer (~21 000 molecules), from which the encapsulation efficiency of Triton X-100 on the CP-dot surfaces was calculated to be 5.5 molecules/nm^2. However, it is difficult to estimate the encapsulation efficiency of Triton X-100 on the CP-dot before dialysis (i.e., 50 nm particles), since the amount of Triton X-100 on such particles could not be detected accurately by UV absorption (i.e., outermost layer of Triton X-100 was not stable and could be dissolved into water) during dialysis. Figure S2 (Supporting Information) also suggests that the immobilized Triton X-100 monolayer on the surface of CP-dots (formed in 64 h after dialysis beginning) was quite stable since their characteristic UV peak at 275 nm did not change upon further dialysis (see the UV spectrum at 72 h).

The UV−vis absorption spectrum and excitation and emission fluorescence spectra of the obtained MEH-PPV CP-dots (solid lines in Figure 1C) have been measured and compared with those of MEH-PPV polymer in THF (dashed lines in Figure 1C). The CP-dots have a wide UV absorption band between 400 and 600 nm with a maximum absorbance at 520 nm. The excitation fluorescence spectrum of the CP-dots has a very similar profile as the UV spectrum and has the maximum fluorescence emission at 520 nm excitation. The CP-dots have a relatively narrow emission fluorescence spectrum with a maximum emission at 590 nm. By comparison, it can be known that the shapes of the spectra (UV absorption spectrum, excitation and emission fluorescence spectra) of the CP-dots are very similar to those of MEH-PPV polymer in organic solvent (dashed lines in Figure 1C). However,the CP-dots in aqueous solution have obvious red-shifts in spectra (20−25 nm) compared with MEH-PPV polymer in THF. The latter has maximum values at 500, 500, and 565 nm, respectively, for UV−vis absorption, excitation fluorescence, and emission fluorescence spectra. The photos of the polymer THF solution and CP-dots aqueous solution are, respectively, orange and pink under white light, whereas they are bright yellow and dark pink under a UV (365 nm) light (inset of Figure 1C). The red-shifts in UV−vis and fluorescence spectra may be attributed to an increase in chain−chain interaction and a conversion of a disorder phase to a highly ordered phase upon swelling of the rapidly reprecipitated nanoparticles with solvent.[13]

Electrochemical and ECL Responses of MEH-PPV CP-Dots. Electrochemical and ECL properties of MEH-PPV CP-dots were investigated on the modified glassy carbon (GC) electrode in aqueous solutions. In the experiment, the CP-dots immobilized-GC electrode was inserted into an ECL cell containing a nitrogen-saturated (or oxygen-free)-phosphate solution (pH 9.0) and applied a cyclic potential between −1.2 and +1.3 V. In the anodic process, CP-dots give an irreversible anodic peak at +0.65 V (curve (a) in Figure 2A), showing that positive charges (holes) can be easily injected into the semiconductive CP-dots. However, in the cathodic process, no obvious cathodic peak can be found, indicating that it is difficult to inject electrons into CP-dots. Without the addition of coreactants, such as TPrA and $S_2O_8^{2-}$, CP-dots only have a weak anodic ECL peak at potential +0.90 V. The weak anodic

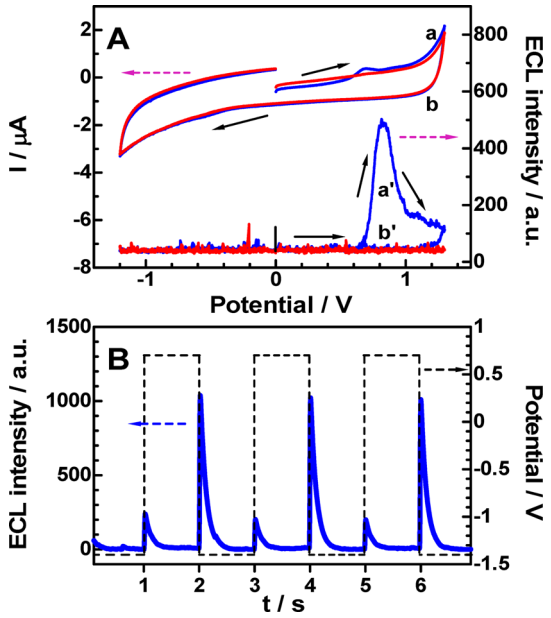

Figure 2. (A) Cyclic voltammogram (CV) and I_{ECL}−V response obtained for the CP-dots in aqueous solution: (a) CV for the CP-dots-modified GC electrode; (b) CV for bare GC electrode; (a′) I_{ECL}−V curve for the CP-dots-modified GC electrode; (b′) I_{ECL}−V curve for the bare GC electrode. (B) Annihilation ECL emission (solid line) obtained for the CP-dots-modified GC electrode in the aqueous solution by stepping potential between +0.7 and −1.4 V (dashed line). The aqueous solution was nitrogen-saturated (i.e., O_2-free) pH 9 phosphate buffer solution.

DOI: 10.1021/acsami.5b04305
ACS Appl. Mater. Interfaces 2015, 7, 15160−15167

ECL may be due to the presence of some impurities in solution,[33] such as OH^- dissociated from water that act as ECL coreactants.[34] Similar weak anodic ECL peaks have been observed for molecular luminophores (e.g., $Ru(bpy)_3^{2+}$),[34] and nanomaterials (e.g., carbon-dots),[35] in neutral or weakly alkaline solutions without adding coreactants.

Annihilation ECL activity of CP-dots was evaluated by recording ECL transients of the nanoparticles upon applying a 1 Hz potential step between anodic and cathodic potentials. A typical ECL response obtained at applying a pulse potential between −1.4 and +0.7 V is shown in Figure 2B. CP-dots give an obvious anodic ECL signal when the potential is stepped from −1.4 to +0.7 V, whereas they give a much higher (4 times) cathodic ECL signal when the potential is stepped from +0.7 V back to −1.4 V. These ECL transients suggest that CP-dots have strong annihilation ECL activity. The possible annihilation ECL mechanism is proposed in eqs 1−3

$$\mathrm{CPD} + \mathrm{e}^- \xrightarrow{k_c} \mathrm{CPD}^- \tag{1}$$

$$\mathrm{CPD} + \mathrm{h}^+ \xrightarrow{k_a} \mathrm{CPD}^+ \tag{2}$$

$$\mathrm{CPD}^- + \mathrm{CPD}^+ \xrightarrow{k_L} \mathrm{CPD}^* + \mathrm{CPD} \rightarrow 2\mathrm{CPD} + h\nu \tag{3}$$

where CPD and CPD* are ground-state and excited-state CP-dots, respectively. In the annihilation ECL process, negatively charged CP-dots (CPD^-) are electrogenerated at a cathodic potential with a rate constant of k_c eq 1), whereas positively charged CP-dots (CPD^+) are produced at an anodic potential with a rate constant of k_a (eq 2. The values of k_c *and* k_a reflect electron- and hole-injection efficiencies, respectively. The annihilation electron transfer between CPD^- and CPD^+ results in the formation of excited-state CP-dots (with a constant rate of k_L), followed by the annihilation ECL emission eq 3. Apparently, the annihilation ECL intensity (or the formation of excited-state of CPD*) is dependent on the rate constants of the electrochemical and chemical steps shown in eqs 1−3 (i.e., k_c, k_a, and k_L). Simultaneously, the lifetimes (or stabilities) of CPD^- and CPD^+ intermediates should influence the ECL emission since CPD^- and CPD^+ are produced sequentially on the electrode by applying double step potentials. The degradation of CPD^- and CPD^+ can be expressed as follows:

$$\mathrm{CPD}^- \xrightarrow{k_1} \text{Product 1} \tag{4}$$

$$\mathrm{CPD}^+ \xrightarrow{k_2} \text{Product 2} \tag{5}$$

The less stable intermediate (CPD^- or CPD^+) will have a larger degradation rate constant (k_1 *or* k_2). It is assumed that the chemiluminescence reaction process, eq 3, is the rate-determining step, i.e., the slowest step in the above ECL reactions; then from eqs 1−5, we can obtain the following net formation rate of CPD^-, CPD^+, and CPD* (see eqs 6−8):

$$\upsilon_{\mathrm{CPD}^-} = \frac{\mathrm{d}[\mathrm{CPD}^-]}{\mathrm{d}t} = k_c\cdot[\mathrm{CPD}] - k_1\cdot[\mathrm{CPD}^-] \tag{6}$$

$$\upsilon_{\mathrm{CPD}^+} = \frac{\mathrm{d}[\mathrm{CPD}^+]}{\mathrm{d}t} = k_a\cdot[\mathrm{CPD}] - k_2\cdot[\mathrm{CPD}^+] \tag{7}$$

$$\upsilon_{\mathrm{CPD}^*} = \frac{\mathrm{d}[\mathrm{CPD}^*]}{\mathrm{d}t} = k_L\cdot[\mathrm{CPD}^-]\cdot[\mathrm{CPD}^+] \tag{8}$$

It is assumed that the concentration of CPD (i.e., [CPD]) does not change during a very short time of electrolysis (e.g., less than 1 s). Then, from eqs 6 and 7, we can obtain the amount of electrogenerated CPD^- and CPD^+, as shown in eqs 9 and 10:

$$[\mathrm{CPD}^-] = \frac{k_c}{k_1}\cdot[\mathrm{CPD}]\cdot(1 - \exp(-k_1 t)) \tag{9}$$

$$[\mathrm{CPD}^+] = \frac{k_a}{k_2}\cdot[\mathrm{CPD}]\cdot(1 - \exp(-k_2 t)) \tag{10}$$

After being applied with the cathodic potential (e.g., −1.4 V) for τ seconds to generate CPD^-, the working electrode is stepped to the anodic potential (e.g., +0.7 V) to produce CPD^+, a sharp anodic ECL peak can be observed in a very short time of t_s ($\ll\tau$). During the follow-up anodic process, the electrogeneration of CPD^- (eq 1) stops and degradation of CPD^- (eq 4 continues, while both electrogeneration and degradation of CPD^+ take place. At the anodic ECL peak ($t = t_s$), the concentrations of CPD^- and CPD^+ (i.e. $[\mathrm{CPD}^-]_{t_s}^{c\rightarrow a}$ and $[\mathrm{CPD}^+]_{t_s}^{c\rightarrow a}$) can be expressed by eqs 11 and 12:

$$[\mathrm{CPD}^-]_{t_s}^{c\rightarrow a} = \frac{k_c}{k_1}\cdot[\mathrm{CPD}]\cdot(1 - \exp(-k_1\tau))\cdot\exp(-k_1 t_s) \tag{11}$$

$$[\mathrm{CPD}^+]_{t_s}^{c\rightarrow a} = \frac{k_a}{k_2}\cdot[\mathrm{CPD}]\cdot(1 - \exp(-k_1 t_s)) \tag{12}$$

Combining eq 8 with eqs 11 and 12, we can obtain eq 13 to estimate the anodic ECL peak:

$$\upsilon_{\mathrm{CPD}^*}^{c\rightarrow a} = \frac{\mathrm{d}[\mathrm{CPD}^*]}{\mathrm{d}t} = \frac{k_L\cdot k_c\cdot k_a}{k_1\cdot k_2}\cdot[\mathrm{CPD}]^2\cdot(1 - \exp(-k_1\tau))\cdot \exp(-k_1 t_s)\cdot(1 - \exp(-k_2 t_s)) \tag{13}$$

Similarly, we can obtain eq 14 to estimate the cathodic ECL peak:

$$\upsilon_{\mathrm{CPD}^*}^{a\rightarrow c} = \frac{\mathrm{d}[\mathrm{CPD}^*]}{\mathrm{d}t} = \frac{k_L\cdot k_c\cdot k_a}{k_1\cdot k_2}[\mathrm{CPD}]^2\cdot(1 - \exp(-k_2\tau))\cdot \exp(-k_2 t_s)\cdot(1 - \exp(-k_1 t_s)) \tag{14}$$

The ratio of anodic ECL peak height to cathodic ECL peak height can be obtained by eq 15:

$$\begin{aligned} R &= \frac{\upsilon_{\mathrm{CPD}^*}^{c\rightarrow a}}{\upsilon_{\mathrm{CPD}^*}^{a\rightarrow c}} \\ &= \frac{(1 - \exp(-k_1\tau))\cdot\exp(-k_1 t_s)\cdot(1 - \exp(-k_2 t_s))}{(1 - \exp(-k_2\tau))\cdot\exp(-k_2 t_s)\cdot(1 - \exp(-k_1 t_s))} \\ &= \frac{k_2}{k_1}\cdot\frac{(1 - \exp(-k_1\tau))}{(1 - \exp(-k_2\tau))} \quad (\text{for } t_s \rightarrow 0) \end{aligned} \tag{15}$$

Equation 15 suggests that the ratio of anodic to cathodic peak height (R) is mainly determined by stabilities of CPD^- and CPD^+ (k_1 and k_2) and is independent of both electron injection efficiency (k_c) and hole injection efficiency (k_a). From eq 15, we can have the following deductions: (1) When $k_2 > k_1$, i.e., CPD^- is more stable than CPD^+, then $R > 1$ (see Figure S4 and related analysis at page S4 in the Supporting Information); i.e., anodic annihilation ECL is stronger than the cathodic one. (2) When $k_2 < k_1$, i.e., CPD^+ is more stable than CPD^-, then $R < 1$; i.e., cathodic annihilation ECL is stronger than the anodic one. On the basis of the above theoretical analysis for

DOI: 10.1021/acsami.5b04305
ACS Appl. Mater. Interfaces 2015, 7, 15160−15167

annihilation ECL reaction kinetics and the fact that cathodic annihilation ECL of CPD is stronger than the anodic one (Figure 2B), we can conclude that CPD^+ is more stable than CPD^-.

The coreactant ECL of CP-dots, including anodic and cathodic ECL, was investigated. The anodic ECL of CP-dots was measured by applying an anodically polarized potential from 0 to +1.3 V in the presence of TPrA (a classic electron donor). A strong anodic ECL signal can be observed for CP-dots in the presence of TPrA at a potential higher than +0.9 V (curve (a) in Figure 3B), with a maximum value at +1.1 V. The

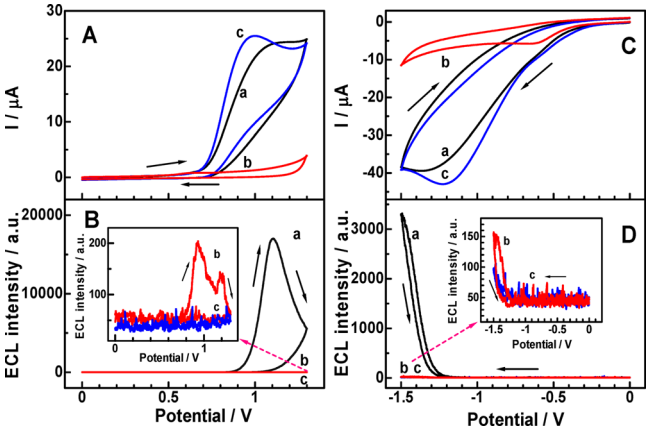

Figure 3. (A) Cyclic voltammograms and (B) anodic ECL responses obtained at GC electrode for systems containing: (a) CP-dots and 5 mM TPrA; (b) CP-dots only; (c) 5 mM TPrA only. Inset: amplified curves b and c. (C) Cyclic voltammograms and (D) cathodic ECL responses obtained at GC electrode for systems containing: (a) CP-dots and 5 mM $K_2S_2O_8$; (b) CP-dots only; (c) 5 mM $K_2S_2O_8$ only. Inset: amplified curve of b and c. The aqueous solutions were pH 9 PBS (0.1 M phosphate). Scan rate was 100 mV s^{-1}.

intensity of the anodic ECL signal from the CP-dots/TPrA system is >100 times stronger than that from a system containing CP-dots only (curve (b) in Figure 3B) or TPrA only (curve (c) in Figure 3B). Apparently, the ECL peak potential (+1.1 V) is much higher than the anodic peak potential (or hole-injection potential) of CP-dots (+0.65 V, curve (b) in Figure 3A) but very near the oxidation peak potential of TPrA (+1.05 V at CP-dots-modified GCE, curve (a); or +0.95 V at bare GCE, curve (c) in Figure 3A). This indicates that hole-bearing CPD^+ (or positively charged CP-dots) at lower anodic potential is quite stable, and its lifetime is longer enough for its further ECL reactions with the electron-donating free radical ($TPrA^\bullet$) electrogenerated from TPrA at higher potential. Moreover, it can be known that anodic ECL potential is determined by the oxidation potential of TPrA. The possible anodic ECL mechanism is proposed in eqs 16−18:

$$CPD - e^- \rightarrow CPD^+ \quad (16)$$

$$TPrA - e^- \rightarrow TPrA^\bullet + H^+ \quad (17)$$

$$CPD^+ + TPrA^\bullet \rightarrow CPD^* + \text{product} \rightarrow CPD + h\nu \quad (18)$$

The cathodic ECL of CP-dots was measured by applying a cathodically polarized potential from 0 to −1.5 V in the presence of $K_2S_2O_8$ (a classic hole donor). A strong cathodic ECL signal can be seen at potentials less than −1.25 V (curve (a) in Figure 3D). The cathodic ECL intensity increases with negatively shifting potential and tends to reach a constant value at potential lower than −1.5 V. It can be known from the comparison of ECL curves in Figure 3D and cyclic voltammograms in Figure 3C that the cathodic ECL that occurs at potentials of −1.25 to −1.5 V is much more negative than the reduction potential of $S_2O_8^{2-}$, i.e., the hole generation potential (begins at −0.6 V and reaches a maximum at −1.2 V). This indicates that the cathodic ECL emission potential is determined by the electron injection potential of CP-dots. Although it is difficult to measure the electron injection potential of CP-dots from CV (curve (b) in Figure 3C) for the absence of current wave, its value can be estimated to be ca. −1.5 V from the ECL potential of CP-dots/$S_2O_8^{2-}$ system (curve (a) in Figure 3D). It should be noted here that the cathodic peaks at −0.6 V (curves (a−c) in Figure 3D) are associated with the reduction of dissolved oxygen. On the basis of the above experimental results, the possible anodic ECL mechanism is proposed in eqs 19−21:

$$S_2O_8^{2-} + e^- \rightarrow SO_4^{\bullet -} + SO_4^{2-} \quad (19)$$

$$CPD + e^- \rightarrow CPD^- \quad (20)$$

$$CPD^- + SO_4^{\bullet -} \rightarrow CPD^* + SO_4^{2-} \rightarrow CPD + h\nu \quad (21)$$

Effect of Trion-X 100 on the ECL Activity of CP-Dots. The nonionic surfactant, Triton X-100, plays an important role in the electrochemistry and ECL of the CP-dots. The Triton X-100-capped CP-dots have an obvious anodic CV peak at +0.65 V (see curve (a) in Figure 4A) and an ECL peak at +0.90 V

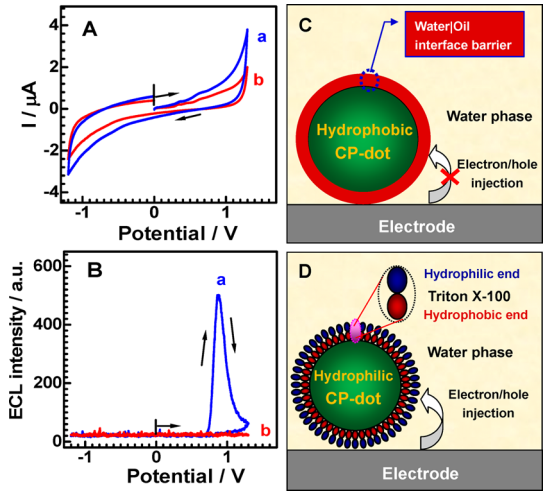

Figure 4. Cyclic voltammograms (A) and ECL responses (B) obtained for Triton X-100-capped CP-dots (a) and bared CP-dots at GC electrodes in nitrogen-saturated (i.e., O_2-free) aqueous solutions (0.1 mol L^{-1} phosphate, pH 9). Schematic models for the electron and hole injections into hydrophobic (C) and hydrophilic (D) CP-dots.

(see curve (a) in Figure 4B), whereas the bare CP-dots do not give any CV or ECL peak (see curve (b) in Figure 4A and curve (b) in Figure 4B, respectively). Apparently, the higher polarity of nanoparticles benefits ECL reactions of CP-dots. The bare MEH-PPV CP-dots are hydrophobic nanoparticles; thus, there will be an oil/water interface between the CP-dots and hydrophilic PBS when they are immobilized on the electrode and inserted into the test aqueous solution (Figure 4C). The formed oil/water interface prevents the electron or hole injection from electrodes, and electrode/hole donors in the hydrophilic phase into the hydrophobic CP-dots, and thus

DOI: 10.1021/acsami.5b04305
ACS Appl. Mater. Interfaces 2015, 7, 15160−15167

blocks the ECL reactions, eqs 1−3 and 16−21, mentioned above. In contrast, Triton X-100-capped CP-dots are hydrophilic nanoparticles (Figure 4D); hence, no oil/water interface is formed between the nanoparticles and hydrophilic phase, and then charge (electron or hole) transfers and ECL reactions can undergo. Generally, the increase in polarity of nanoparticles may enhance the solubility of nanoparticles in water. Therefore, the stability of Triton X-100-capped CP-dots film at the GC electrode surface was investigated by immersing the modified electrode for different times. It was found that ECL intensity had a slight decrease in ECL (ca. 10%) upon the first 20 min immersing and maintained a relatively constant value with further immersing (Figure S5, Supporting Information), showing that Triton X-100-capped CP-dots film is basically stable at the GC electrode. The satisfied stability might be attributed to the nonionic property of Triton X-100 and possible hydrogen bonds between the hydrophilic poly(ethylene oxide) chain and −COOH and −OH groups at GC electrode surfaces. The effects of other surfactants, including poly(styrene-*co*-maleic anhydride) (PSMA), Pluronic F-127, and sodium dodecyl sulfate (SDS), were investigated. The former two surfactants are amphiphilic polymers (or nonionic surfactants), and the latter is a typical ionic surfactant. Experimental results show that the ECL activities of the MEH-PPV dots capped by PSMA or Pluronic F-127 are much weaker than that of CP-dots capped with Triton X-100 (Figure S6, Supporting Information). In terms of the ionic surfactants, such as SDS, we have had tried to prepare and investigate CP-dots capped by these types of surfactants. However, we failed to do this because SDS has poor solubility in THF and the reprecipitation method is not appropriate for preparing CP-dots capped by SDS. Briefly, the preparation of Triton X-100 functionalized hydrophilic CP-dots realizes the strong ECL emissions of the emerging CP-dots in aqueous solution.

Effect of Electrode Material on ECL of CP-Dots, and ECL Spectra. Electrode material strongly affects the ECL of the CP-dots. Three working electrodes of different materials, including GC, Pt, and Au, were used to investigate the ECL responses of CP-dots, respectively. The cathodic and anodic ECL peak intensities obtained at different working electrodes are compared and shown in Figure 5A,C. Both cathodic and anodic ECL intensities obtained at the GC electrode are much higher than those obtained at Pt and Au electrodes, with the order: GC ≫ Au > Pt. The significant difference in ECL activity of CP-dots at the different working electrodes may be associated with the polarity of the working electrode. It has been reported that Pt and Au electrode surfaces are quite hydrophilic, whereas the GC electrode has a relatively hydrophobic surface.[36] Although Triton X-100-capped CP-dots are hydrophilic, their polarity (determined by the poly(ethylene oxide) chain of Triton X-100 after capping) is relatively low. Therefore, Triton X-100-capped CP-dots may have better electrochemical and ECL activities at the GC electrode with relatively lower polarity.

The spectra of cathodic and anodic ECL emissions at GC electrodes were measured and are shown in Figure 5B,D, respectively. The ECL spectra from the cathode and anode (black columns) are very similar, with maximum ECL emission peaks at 590 nm, suggesting that the cathodic ECL of the CP-dots/$S_2O_8^{2-}$ system and the anodic ECL of CP-dots/TPrA share the same ECL luminophores. Moreover, the ECL spectra of CP-dots are essentially the same as their FL emission spectra with a maximum intensity at 590 nm (red dashed lines in Figure 5B,D), indicating that ECL of CP-dots involves a nonsurface state ECL reaction mechanism.[33,37−39] In other words, ECL and FL of CP-dots share the same ground and excited states.

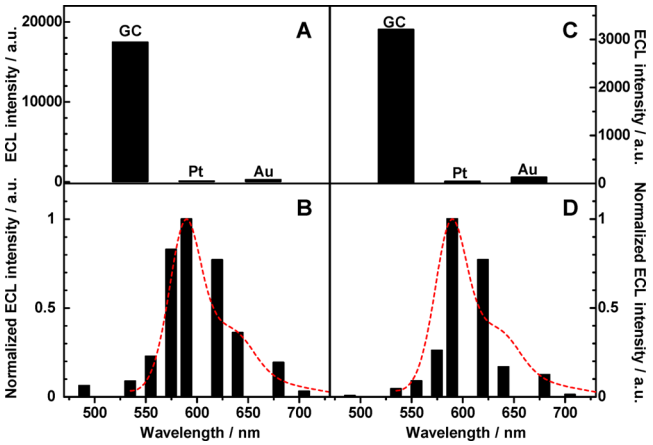

Figure 5. Anodic (A) and cathodic (C) ECL peak intensities obtained for CP-dots−coreactant systems at different kinds of electrodes. Anodic (B) and cathodic (D) ECL spectra obtained for CP-dots−coreactant systems at the GC electrodes. The coreactants in anodic and cathodic CP-dots−coreactant ECL systems were 5 mM TPrA and 5 mM $K_2S_2O_8$, respectively. For comparison with ECL spectra of CP-dots, the fluorescence emission spectra of CP-dots (red dashed lines) were provided in (B) and (D).

Effect of Dissolved Oxygen. It is well-known that dissolved O_2 is an important quencher to the fluorescence and ECL of luminophores, such as $Ru(bpy)_3^{2+}$, via energy transfer from the excited state of luminophores to O_2. Thus, the effect of dissolved O_2 in aqueous solution on the ECL of CP-dots was investigated. For the anodic ECL including annihilation ECL (Figure S7, Supporting Information) and the coreactant anodic ECL in the presence of TPrA (Figure S8, Supporting Information), their emissions are obviously inhibited and their intensity are decreased with increasing dissolved O_2 concentration in samples (i.e., using N_2 (O_2 free)-, air (20% O_2)-, and pure O_2 (100% O_2)-saturated PBS in turn). Apparently, this ECL inhibition can be attributed to the quenching of excited-state CP-dots by O_2. However, for cathodic ECL of CP-dots, including annihilation and coreactant ECL routes, dissolved O_2 has both enhancing and quenching effects (Figures S7 and S9, Supporting Information). In the presence of relatively low O_2 concentration (i.e., in air-saturated solution), dissolved O_2 can enhance the ECL of CP-dots. This enhancement of ECL implies that O_2 might act as a coreactant, or electron transfer mediator, although the exact enhancing mechanism is unknown in the present stage. In the presence of high O_2 concentration (i.e., in pure O_2-saturated solution), ECL is obviously inhibited compared with the case of O_2-free (i.e., N_2-saturated solution), suggesting that the above-mentioned quenching effect of O_2 (via energy transfer from the excited state of CP-dots to O_2) on the ECL CP-dots is dominant at high O_2 concentration.

ECL Mechanism. On the basis of the above experimental results and discussion, the ECL mechanisms of CP-dots are summarized in Figure 6. The hydrophilic Triton X-100-capped CP-dots have an optical band gap of 2.1 eV (590 nm) in aqueous solution. At the GC electrode, the hydrophilic CP-dots can easily obtain electrons and holes from the electrode directly or from electrogenerated free radicals and give ECL emission

DOI: 10.1021/acsami.5b04305
ACS Appl. Mater. Interfaces 2015, 7, 15160−15167

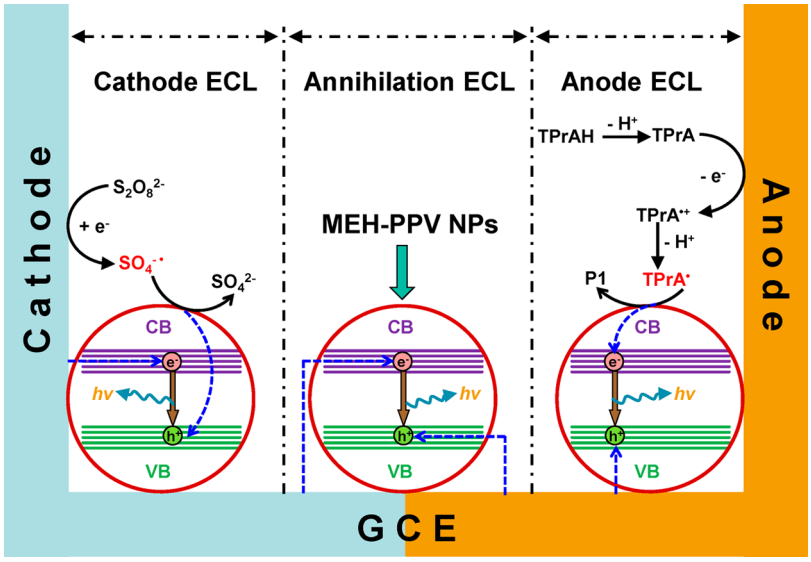

Figure 6. Proposed ECL reaction mechanisms for CP-dots in aqueous solutions.

via three types of ECL routes. In the annihilation ECL route, electrons and holes are all provided directly by the working electrode.

The electrons and holes are injected, respectively, into the conduction band (CB) and valence band (VB) of the CP-dots by applying a stepping potential; i.e., the GC working electrode is periodically switched between anode and cathode. The subsequent annihilation of the electron/hole pairs gives rise to ECL emission. In the anodic ECL route, holes are injected into the VB of CP-dots directly by the anode, whereas electrons are injected into the CB of CP-dots by the anodically generated $TPrA^{\bullet}$ radicals, which is followed by the annihilation of electrons and holes, and anodic ECL emission. In the cathodic ECL route, electrons are provided directly by the cathode, whereas holes are donated by the cathodically generated $SO_4^{\bullet-}$ free radicals. The annihilation of electrons and holes in the CP-dots produce the cathodic ECL emission.

4. CONCLUSIONS

In summary, hydrophilic and strongly ECL CP-dots have been synthesized by capping hydrophobic MEH-PPV CP-dots with the nonionic surfactant Triton X-100. For the first time, the ECL of CP-dots was investigated in aqueous solution. The hydrophilic CP-dots exhibit annihilation ECL, anodic ECL, and cathodic coreactant ECL activities at the GC working electrode. The nonsurface state ECL and easily tunable band gap of the semiconducting polymer enable the synthesis and applications of multicolor CP-dots. Additionally, CP-dots possess low cytotoxicity, good biocompatibility, and easy labeling and bioconjugation, suggesting that the hydrophilic CP-dots are a new type of excellent ECL nanomaterial as semiconducting nanocrystals, carbon quantum dots. It is envisioned that the hydrophilic CP-dots have promising applications in novel chemosensing, biosensing, and new types of light-emitting diodes. For examples, the sensitive anodic ECL response with TPrA implies that the hydrophilic CP-dots might be used to develop chemical sensors for some biologically interesting molecules such as amino acids, proteins, or amine-containing drugs. The easy modification of the CP-dots on electrodes might enable the development of new types of label-free solid-state ECL immunosensors for antibodies or antigens. The ECL emission might enable fabrication of new types of orange (590 nm) light-emitting devices, the light emission of which could be controlled by various stimulating potential signals (e.g., pulse, constant, or scanning potentials) and different molecules (e.g., charge or hole donors).

■ ASSOCIATED CONTENT

Supporting Information

Figures S1−S8. The Supporting Information is available free of charge on the ACS Publications website at DOI: 10.1021/acsami.5b04305.

■ AUTHOR INFORMATION

Corresponding Author

*E-mail: y.w.chi@fzu.edu.cn. Tel/Fax: +86-591-22866137.

Author Contributions

The manuscript was written through contributions of all authors. All authors have given approval to the final version of the manuscript.

Notes

The authors declare no competing financial interest.

■ ACKNOWLEDGMENTS

This study was financially supported by the National Natural Science Foundation of China (21375020), the Specialized Research Fund for the Doctoral Program of Higher Education of China (20133514110001), and the Program for Changjiang Scholars and Innovative Research Team in University (No. IRT1116).

■ ABBREVIATIONS

MEH-PPV, poly[2-methoxy-5-(2-ethylhexyloxy)-1,4-phenylenevinylene]
CP, conjugated polymer
ECL, electrochemiluminescence or electrochemiluminescent
TPrA, tri-*n*-propylamine
THF, tetrahydrofuran
CV, cyclic voltammogram or cyclic voltammetry
CPD, CP-dots
CB, conduction band

DOI: 10.1021/acsami.5b04305
ACS Appl. Mater. Interfaces 2015, 7, 15160−15167

VB, valence band

REFERENCES

(1) Grimsdale, A. C.; Chan, K. L.; Martin, R. E.; Jokisz, P. G.; Holmes, A. B. Synthesis of Light-Emitting Conjugated Polymers for Applications in Electroluminescent Devices. *Chem. Rev.* **2009**, *109*, 897−1091.

(2) Friend, R. H.; Gymer, R. W.; Holmes, A. B.; Burroughes, J. H.; Marks, R. N.; Taliani, C.; Bradley, D. D. C.; Dos Santos, D. A.; Brédas, J. L.; Lögdlund, M.; Salaneck, W. R. Electroluminescence in Conjugated Polymers. *Nature* **1999**, *397*, 121−128.

(3) Günes, S.; Neugebauer, H.; Sariciftci, N. S. Conjugated Polymer-Based Organic Solar Cells. *Chem. Rev.* **2007**, *107*, 1324−1338.

(4) Piok, T.; Gamerith, S.; Gadermaier, C.; Plank, H.; Wenzl, F. P.; Patil, S.; Montenegro, R.; Kietzke, T.; Neher, D.; Scherf, U.; Landfester, K.; List, E. J. W. Organic Light-Emitting Devices Fabricated from Semiconducting Nanospheres. *Adv. Mater.* **2003**, *15*, 800−804.

(5) Landfester, K.; Montenegro, R.; Scherf, U.; Güntner, R.; Asawapirom, U.; Patil, S.; Neher, D.; Kietzke, T. Semiconducting Polymer Nanospheres in Aqueous Dispersion Prepared by a Miniemulsion Process. *Adv. Mater.* **2002**, *14*, 651−655.

(6) Wu, C.; Chiu, D. T. Highly Fluorescent Semiconducting Polymer Dots for Biology and Medicine. *Angew. Chem., Int. Ed.* **2013**, *52*, 3086−3109.

(7) Childress, E. S.; Roberts, C. A.; Sherwood, D. Y.; LeGuyader, C. L. M.; Harbron, E. J. Ratiometric Fluorescence Detection of Mercury Ions in Water by Conjugated Polymer Nanoparticles. *Anal. Chem.* **2012**, *84*, 1235−1239.

(8) Ye, F.; Wu, C.; Jin, Y.; Chan, Y.; Zhang, X.; Chiu, D. T. Ratiometric Temperature Sensing with Semiconducting Polymer Dots. *J. Am. Chem. Soc.* **2011**, *133*, 8146−8149.

(9) Cordovilla, C.; Swager, T. M. Strain Release in Organic Photonic Nanoparticles for Protease Sensing. *J. Am. Chem. Soc.* **2012**, *134*, 6932−6935.

(10) Feng, X.; Lv, F.; Liu, L.; Tang, H.; Xing, C.; Yang, Q.; Wang, S. Conjugated Polymer Nanoparticles for Drug Delivery and Imaging. *ACS Appl. Mater. Interfaces* **2010**, *2*, 2429−2435.

(11) Fernando, L. P.; Kandel, P. K.; Yu, J.; McNeill, J.; Ackroyd, P. C.; Christensen, K. A. Mechanism of Cellular Uptake of Highly Fluorescent Conjugated Polymer Nanoparticles. *Biomacromolecules* **2010**, *11*, 2675−2682.

(12) Sun, B.; Sun, M.; Gu, Z.; Shen, Q.; Jiang, S.; Xu, Y.; Wang, Y. Conjugated Polymer Fluorescence Probe for Intracellular Imaging of Magnetic Nanoparticles. *Macromolecules* **2010**, *43*, 10348−10354.

(13) Pecher, J.; Mecking, S. Nanoparticles of Conjugated Polymers. *Chem. Rev.* **2010**, *110*, 6260−6279.

(14) Landfester, K.; Montenegro, R.; Scherf, U.; Güntner, R.; Asawapirom, U.; Patil, S.; Neher, D.; Kietzke, T. Semiconducting Polymer Nanospheres in Aqueous Dispersion Prepared by a Miniemulsion Process. *Adv. Mater.* **2002**, *14*, 651−655.

(15) Howes, P.; Thorogate, R.; Green, M.; Jickells, S.; Daniel, B. Synthesis, Characterisation and Intracellular Imaging of PEG Capped BEHP-PPV Nanospheres. *Chem. Commun.* **2009**, 2490−2492.

(16) Hashim, Z.; Howes, P.; Green, M. Luminescent Quantum-Dot-Sized Conjugated Polymer Nanoparticles—Nanoparticle Formation in a Miniemulsion System. *J. Mater. Chem.* **2011**, *21*, 1797−1803.

(17) Li, Y.; Liu, J.; Liu, B.; Tomczak, N. Highly Emissive PEG-encapsulated Conjugated Polymer Nanoparticles. *Nanoscale* **2012**, *4*, 5694−5702.

(18) Szymanski, C.; Wu, C.; Hooper, J.; Salazar, M. A.; Perdomo, A.; Dukes, A.; McNeill, J. Single Molecule Nanoparticles of the Conjugated Polymer MEH−PPV, Preparation and Characterization by Near-Field Scanning Optical Microscopy. *J. Phys. Chem. B* **2005**, *109*, 8543−8546.

(19) Wu, C.; Szymanski, C.; Cain, Z.; McNeill, J. Conjugated Polymer Dots for Multiphoton Fluorescence Imaging. *J. Am. Chem. Soc.* **2007**, *129*, 12904−12905.

(20) Wu, C.; Bull, B.; Szymanski, C.; Christensen, K.; McNeill, J. Multicolor Conjugated Polymer Dots for Biological Fluorescence Imaging. *ACS Nano* **2008**, *2*, 2415−2423.

(21) Wu, C.; Schneider, T.; Zeigler, M.; Yu, J.; Schiro, P. G.; Burnham, D. R.; McNeill, J. D.; Chiu, D. T. Bioconjugation of Ultrabright Semiconducting Polymer Dots for Specific Cellular Targeting. *J. Am. Chem. Soc.* **2010**, *132*, 15410−15417.

(22) Wu, C.; Jin, Y.; Schneider, T.; Burnham, D. R.; Smith, P. B.; Chiu, D. T. Ultrabright and Bioorthogonal Labeling of Cellular Targets Using Semiconducting Polymer Dots and Click Chemistry. *Angew. Chem., Int. Ed.* **2010**, *49*, 9436−9440.

(23) Wu, C.; Hansen, S. J.; Hou, Q.; Yu, J.; Zeigler, M.; Jin, Y.; Burnham, D. R.; McNeill, J. D.; Olson, J. M.; Chiu, D. T. Design of Highly Emissive Polymer Dot Bioconjugates for In Vivo Tumor Targeting. *Angew. Chem., Int. Ed.* **2011**, *50*, 3430−3434.

(24) Yu, J.; Wu, C.; Zhang, X.; Ye, F.; Gallina, M. E.; Rong, Y.; Wu, I.; Sun, W.; Chan, Y.; Chiu, D. T. Stable Functionalization of Small Semiconducting Polymer Dots via Covalent Cross-Linking and Their Application for Specific Cellular Imaging. *Adv. Mater.* **2012**, *24*, 3498−3504.

(25) Chan, Y.-H.; Wu, P.-J. Semiconducting Polymer Nanoparticles as Fluorescent Probes for Biological Imaging and Sensing. *Part. Part. Syst. Charact.* **2015**, *32*, 11−28.

(26) Zhu, C.; Liu, L.; Yang, Q.; Lv, F.; Wang, S. Water-Soluble Conjugated Polymers for Imaging, Diagnosis, and Therapy. *Chem. Rev.* **2012**, *112*, 4687−4735.

(27) Feng, L.; Zhu, C.; Yuan, H.; Liu, L.; Lv, F.; Wang, S. Conjugated Polymer Nanoparticles: Preparation, Properties, Functionalization and Biological Applications. *Chem. Soc. Rev.* **2013**, *42*, 6620−6633.

(28) Chang, Ya.; Palacios, R. E.; Fan, F.; Bard, A. J.; Barbara, P. F. Electrogenerated Chemiluminescence of Single Conjugated Polymer Nanoparticles. *J. Am. Chem. Soc.* **2008**, *130*, 8906−8907.

(29) Nepomnyashchii, A. B.; Ono, R. J.; Lyons, D. M.; Sessler, J. L.; Bielawski, C. W.; Bard, A. J. Oligothiophene Nanoparticles: Photophysical and Electrogenerated Chemiluminescence Studies. *J. Phys. Chem. Lett.* **2012**, *3*, 2035−2038.

(30) Suk, J.; Bard, A. J. Electrochemistry and Electrogenerated Chemiluminescence of Organic Nanoparticles. *J. Solid State Electrochem.* **2011**, *15*, 2279−2291.

(31) Friend, R. H.; Gymer, R. W.; Holmes, A. B.; Burroughes, J. H.; Marks, R. N.; Taliani, C.; Bradley, D. D. C.; Dos Santos, D. A.; Brédas, J. L.; Lögdlund, M.; Salaneck, W. R. Electroluminescence in Conjugaed Polymers. *Nature* **1999**, *397*, 121−128.

(32) Richter, M. M.; Fan, F. F.; Klavetter, F.; Heeger, A. J.; Bard, A. J. *Chem. Phys. Lett.* **1994**, *226*, 115−120.

(33) Myung, N.; Ding, Z.; Bard, A. J. Electrogenerated Chemiluminescence of CdSe Nanocrystals. *Nano Lett.* **2002**, *2*, 1315−1319.

(34) Zheng, L.; Chi, Y.; Shu, Q.; Dong, Y.; Zhang, L.; Chen, G. Electrochemiluminescent Reaction between $Ru(bpy)_3^{2+}$ and Oxygen in Nafion Film. *J. Phys. Chem. C* **2009**, *113*, 20316−20321.

(35) Zheng, L.; Chi, Y.; Dong, Y.; Lin, J.; Wang, B. Electrochemiluminescence of Water-Soluble Carbon Nanocrystals Released Electrochemically from Graphite. *J. Am. Chem. Soc.* **2009**, *131*, 4564−4565.

(36) Zu, Y.; Bard, A. J. Electrogenerated Chemiluminescence. 67. Dependence of Light Emission of the Tris(2,2′) bipyridylruthenium-(II)/Tripropylamine System on Electrode Surface Hydrophobicity. *Anal. Chem.* **2001**, *73*, 3960−3964.

(37) Bae, Y.; Myung, N.; Bard, A. J. Electrochemistry and Electrogenerated Chemiluminescence of CdTe Nanoparticles. *Nano Lett.* **2004**, *4*, 1153−1161.

(38) Ding, Z.; Quinn, B. M.; Haram, S. K.; Pell, L. E.; Korgel, B. A.; Bard, A. J. Electrochemistry and Electrogenerated Chemiluminescence from Silicon Nanocrystal Quantum Dots. *Science* **2002**, *296*, 1293−1297.

(39) Myung, N.; Bae, Y.; Bard, A. J. Effect of Surface Passivation on the Electrogenerated Chemiluminescence of CdSe/ZnSe Nanocrystals. *Nano Lett.* **2003**, *3*, 1053−1055.

DOI: 10.1021/acsami.5b04305
ACS Appl. Mater. Interfaces 2015, 7, 15160−15167